Excited State Structural Dynamics of Tetra(4-aminophenyl)porphine in the Condensed Phase: Resonance Raman Spectroscopy and Density Functional Theory Calculation Study

Huigang Wang,* Jun Xu, Junmin Wan, Yanying Zhao, and Xuming Zheng*

Contribution from the Department of Chemistry and State Key Laboratory of ATMMT(MOE), Zhejiang Sci-Tech University, Hangzhou, People's Republic of China 310018

Received: January 5, 2010; Revised Manuscript Received: February 7, 2010

Resonance Raman spectra (RRs) of tetra(4-aminophenyl) porphine (TAPP) were obtained, and density functional calculations were done to help the elucidation of the photorelaxation dynamics of Soret (B_x and B_y band) and Q_y electronic transitions. The RRs indicate that the photorelaxation dynamics for the $S_0 \rightarrow S_3$ excited electronic state is predominantly along the totally symmetric porphin ring $C_\beta{=}C_\beta + C_mC_\alpha$ stretch, C_m-ph stretch, and simultaneously along the asymmetric $\nu(C_mC_\alpha)_{as}$ and $\nu(C_\alpha C_\beta)_{as}$ relaxation processes leading to Q_y while that for $S_0 \rightarrow S_2$ is predominantly along the porphin ring $C_\beta{=}C_\beta + C_mC_\alpha$ stretch and simultaneously along the asymmetric $\nu(C_mC_\alpha)_{as} + \nu(C_\alpha C_\beta)_{as}$ relaxation processes leading to thermal equilibrium in Q_x. The excited state structural dynamics of TAPP determined from RRs shows that internal conversion $B_x \rightarrow Q_y$ electronic relaxation occurs in tens of femtoseconds and the short-time dynamics were first interpreted with account of the time-dependent wave packet theory and Herzberg−Teller contributions.

Introduction

Numerous biological pigment−protein complexes participating in energy- and charge-transfer processes contain tetrapyrrolic chromophores (chlorophylls, bacteriochlorophylls, bilins) with optical properties appropriate to the two-photon laser scanning fluorescence microscopy, optical power limiting, three-dimensional optical storage, microfabrication, and up-converted lasing.[1−3] Thus, the emulation of the high efficiency characteristic of biological electron-transfer systems becomes a timely topic. However, the design and emulation of such a system depends largely on the understanding and the deep insight to the photophysics of the excitation coupling dynamics, energy/electron transfers, and structural changes in their excited state, especially in relation to natural light-harvesting systems.

The energy/electron transfer, intersystem crossing, and electron localization process in porphyrins and metal complexes have been studied in great detail.[4−10] However, the ultrafast electronic-state dynamics, in particular its short-time evolution between the B and Q_x state, is currently uncertain for ultrafast spectroscopy and forms the subject of much debate.[7−10] Studies employing femtosecond fluorescence depletion[7−9] have indicated that the internal conversions $B \rightarrow Q_y$ and $Q_y \rightarrow Q_x$, starting from vibrationally excited levels of the Soret (or B) band, occur in less than 50 and 100 fs, respectively. Paradoxically, however, line widths measured of the distinct and sharp lines in the absorption spectrum of supersonically cooled, isolated H_2TPP molecules indicate a lifetime of at least 5 ps.[10]

In contrast with the ultrafast electronic spectra, the vibrational spectroscopies such as resonance Raman spectroscopy and infrared absorption are generally capable of revealing detailed information of molecular and electronic structure as well as photo short-time dynamics and vibronic coupling in excited states.[11] An enormous amount of research has been devoted to the use of this technique to study porphyrins.[12−20] A series of papers by Saini et al. used RR and IR spectroscopy to study the character of tetraphenylporphyrin (TPP) and its dication radicals,[12−15] following the work of Binstead et al.[21,22] Bell et al. studied the lowest excited singlet and triplet states of TPP using two-color time-resolved resonance Raman spectroscopy.[16−20] They observed and discussed the significant frequency shifts of the porphyrin core vibrations upon excitation to the S_1 or T_1 state and assigned the ground and triplet state bands, respectively, with the combination of isotope substitution with polarization data.[16−20] Egawa et al. predicted that some higher energy excited states exist for vibronic coupling with the Soret state through the A_{2g} nontotally symmetric mode in iron(II) normal- and hyperporphyrins according to the resonance Raman spectroscopy experiment.[23]

Although resonance Raman spectroscopy has been extensively applied to porphyrin-based materials, surprisingly most of the RR spectroscopy was obtained in a very narrow frequency region and interpreted mostly on fundamental vibrational modes; little work has been carried out on Franck−Condon region short-time dynamic analysis for the vibronic coupling phenomenon which may lead to conical intersection between different potential energy surfaces (PES) and alter the photoreaction channel. In this paper, we report a preliminary resonance Raman analysis of the short-time excited state dynamics of tetra(4-aminophenyl)porphine (TAPP) in its B- and Q-band absorption and find a higher energy excited state that vibronically coupled to the B band.

Computational chemical methods may be carried out to better understand vibrational spectra. A detailed normal-mode analysis for porphin (H_2P) has been carried out and explored the coordinate mixing between the protonated and deprotonated pyrrole rings.[24−26] Minaev et al. investigated the vibrational frequencies and vibronic structure of the first $S_0 \rightarrow S_1$absorption band of H_2P by DFT with the B3LYP functional.[27] Zhang et al. studied the influence of different substitution on the vibrational spectrum and geometry of porhyrin macrocycles.[28] Density functional theory has been proved to be a useful

* To whom correspondence should be addressed. E-mail: zdwhg@163.com (H.W.); xvmingzheng@gmail.com (X.Z.). Phone: 00186-571-8684-3627 (H.W.); 86-571-86843699 (X.Z.). Fax: 00186-571-8684-3627 (H.W.); 86-571-86843702 (X.Z.).

10.1021/jp1000978
Published on Web 02/22/2010

computational tool and been used to study the structure and vibrational frequencies of TAPP related species.[11,12] Time dependent DFT calculations may be used to study the electronic properties of porphrin-based materials.[29] Herein, DFT calculations were carried out using the hybrid B3LYP functional to aid vibrational mode assignments.

In this paper, we report a preliminary resonance Raman study of the short-time excited state dynamics of TAPP in its B absorption. We acquired 397.9, 416, 435.7, and 514 nm resonance Raman spectra in order to characterize the short-time excited state dynamics. We compare the results obtained from different excited states of TAPP and interpret the Herzberg−Teller coupling according to the selection rule of the polarizability tensor.

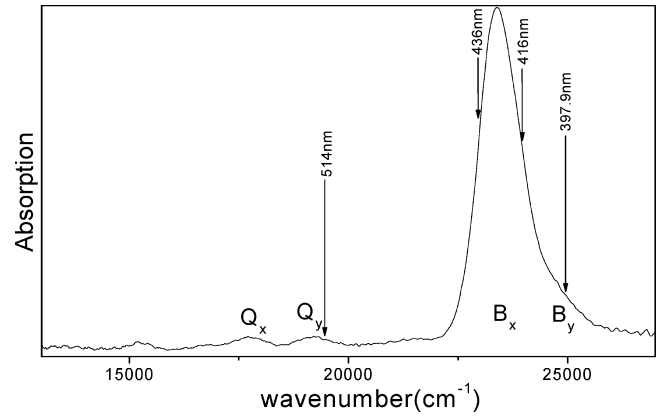

Figure 1. Absorption spectrum of TAPP in dichloromethane solution.

Experimental and Computational Methods

Resonance Raman Experiments. The methods and experimental apparatus used for the resonance Raman experiments have been described elsewhere,[30] so only a short account will be given here. The harmonics of a nanosecond Nd:YAG laser and their hydrogen Raman shifted laser lines were used to generate the 397.9, 416, and 435.7 nm excitation wavelengths employed in the resonance Raman experiments. Since the B-band molar extinction coefficients of TAPP are fairly high, rather low concentrations were used for measurements. The solution-phase samples used concentrations of approximately $10^{-6}-10^{-3}$ M TAPP (99% purity, synthesized and purified by silica-gel column chromatography, the purity was testified with HPLC) in spectroscopic grade dichloromethane (99.5^{+}% purity, Sigma) solvent. A lower power was used during the resonance Raman measurements to avoid saturation effects and other problems associated with high peak powers. High peak power can also produce more photochemical intermediates or cause the two-photon ionization processes to occur during the laser pulse. The excitation laser beam was loosely focused to about a 0.5−1.0 mm diameter spot size onto a flowing liquid stream of sample so as to ensure that all of the Raman peaks belong to the TAPP compound. A backscattering geometry was used for sample excitation and for collection of the Raman scattered light by reflective optics that imaged the Raman scattered light through a polarizer and entrance slit of a 0.5 m spectrograph. The grating of the spectrograph dispersed the light onto a liquid nitrogen cooled charge coupled device (CCD) mounted on the exit of the spectrograph, and the CCD acquired the Raman signal for about 90−150 s before being read out to an interfaced personal computer. About 10−30 of these scans were summed to obtain the resonance Raman spectrum. The Raman shifts of the resonance Raman spectra were calibrated using the known vibrational frequencies of the dichloromethane solvent Raman bands. The solvent Raman bands were subtracted from the resonance Raman spectrum using an appropriately scaled solvent spectrum. The Fourier transform (FT) IR and FT-Raman spectra of TAPP in the neat solid phase were acquired to help assign the resonance Raman spectra.

The spectra of an intensity calibrated deuterium lamp were used to correct the resonance Raman spectrum intensities for the variation in detection efficiency as a function of wavelength, and portions of the resonance Raman spectra were fitted to a baseline plus a sum of Lorentzian bands to find the integrated areas of the Raman bands. The absolute Raman cross sections of the TAPP resonance Raman spectra were determined relative to the 704 cm^{-1} Raman band of dichloromethane. The absolute Raman cross section of dichloromethane was measured from the 918 cm^{-1} absolute Raman cross section of acetonitrile by a 1:1 volume ratio mixture. The 918 cm^{-1} mode of acetonitrile was used as the internal standard for excitation wavelengths above 250 nm. The detailed procedures for determination of absolute resonance Raman cross sections of solutes (acetonitrile) have been adopted from refs 31 and 32. The depolarization ratio of the Raman fundamental for TAPP was determined by passing the incident laser through a calcite Glan-Taylor polarizer to ensure linear polarization, and placing a thin film UV polarization analyzer in the Raman-scattered beam path. The detected polarization was rotated between parallel and perpendicular on successive accumulations. An ultraviolet−visible (UV−vis) spectrometer was used to determine the concentrations of the TAPP sample before and after each measurement; the absorption spectrum changed by <5% due to photodecomposition and/or solvent evaporation, and the absolute Raman cross sections were computed using the average concentration before and after three measurements and finding the mean of three trials to get a final value for the excitation wavelengths determined.

Time-Dependent Wave Packet Calculations. Resonance Raman intensities were modeled using Heller's time-dependent wave packet approach to resonance Raman scattering.[33−36] Resonance Raman intensities were calculated using the following formula:

$$\sigma_R(E_L) = (8\pi e^4 E_S{}^3 E_L M_0{}^4/9\hbar^6 c^4) \int_{-\infty}^{\infty} G(\delta)\, d\delta \times \left| \int_0^{\infty} dt \langle f|0(t)\rangle \exp[i(E_L + \varepsilon_0)t/\hbar] \times \exp[-\Gamma t/\hbar] \right|^2 \quad (1)$$

where E_L is the incident photon energy, ε_0 is the energy of the initial vibrational state, M_0 is the transition length evaluated at the equilibrium geometry, and f is the final state for the Raman scattering. The term $\exp[-\Gamma t/\hbar]$ is a homogeneous damping function that has contributions from the excited state population decay and pure dephasing. $G(\delta)$ is an inhomogeneous distribution of transition energies. $|0(t)\rangle = e^{-iH_v t/\hbar}$, which is the initial multidimensional vibrational state propagated on the excited state surface for a time t and H is the excited state vibrational Hamiltonian.[33,37]

Density functional theory (DFT)[38,39] calculations were done to determine the optimized geometry and vibrational frequencies as well as the electronic transition energies for the ground or excited electronic states of TAPP. Initial geometry optimization was carried out with 6-31G basis sets without symmetry constraint. The obtained structure was adapted with suitable symmetry constraint and then used for final optimization using

TABLE 1: RB3LYP-TD/6-31G(d) Computed Electronic Absorption Spectrum (nm), Electric Dipole Transition Moment *M*, and Oscillator Strength *f* of TAPP (HOMO = MO 177)

singlet state C_{2v}		main CI contributions	M_a[a]		f[a]		nm	
			M	*a*	calcd	exptl	calcd	exptl
S_1	1^1B_1	0.51(176→178) − 0.51(177→179)	0.453	X	0.01	0.03	557.13 (2.2 eV)	565
S_2	1^1B_2	0.57(177→178) + 0.42(176→179)	0.945	Y	0.05	0.05	536.09 (2.3 eV)	521
S_3	2^1B_1	0.41(177→179) + 0.32(176→178)	3.269	X	0.82	1.04	397.49 (3.1 eV)	428
S_4	2^1B_2	0.45(172→178) − 0.32(176→179)	3.290	Y	0.93	0.20	354.72 (3.5 eV)	401

[a] M_a is a projection of the electric dipole transition moment on the *a* axis (au), and *f* is an oscillator strength.

TABLE 2: RB3LYP-TD/6-31G(d) Orbital Energy Levels (in au) and Symmetry Labels of Some of the Highest Occupied and Lowest Unoccupied Orbitals of TAPP

orbital	orbital energies (in au)
LUMO-1(179)	−0.052(B2)
LUMO(178)	−0.063(B1)
HOMO(177)	−0.164(A1)
HOMO-1(176)	−0.165(A2)
HOMO−LUMO	−0.101

6-31G(d) basis sets. Vibration frequencies were computed by using the RB3LYP/6-31G(d) level of theory for the ground state of TAPP with C_{2v} symmetry, while the electronic transition energies were calculated using RB3LYP-TD/6-31G(d). All of the DFT calculations made use of the Gaussian program software suite.[40]

The theory of Raman scattering is provide in the Supporting Information; see also refs 37 and 41.

Results and Discussion

A. Absorption Spectrum. Figure 1 presents the absorption spectrum of tetra(4-aminophenyl)porphine (TAPP) in dichloromethane solution with the wavelengths for the resonance Raman experiments indicated above the spectrum. Table 1 lists the RB3LYP-TD/6-31G(d) computed electronic absorption spectrum, electric dipole transition moment *M*, the corresponding orbitals, and the oscillator strengths for TAPP. Table 1 shows that, among the calculated electronic transitions above the 350 nm optical region, there are four transition-allowed absorption bands at 355 and 397 nm (B_y and B_x band with oscillator strengths of $f = 0.93$ and 0.82, respectively) and 536 and 557 nm (Q_y and Q_x band with oscillator strengths of $f = 0.05$ and 0.01, respectively). This is in good agreement with the intense experimental absorption band at 401 and 428 nm (B_y and B_x band with experimental oscillator strengths of $f = 0.20$ and 1.04, respectively) and 521 nm and 565 nm (Q_y and Q_x band with experimental oscillator strengths of $f = 0.05$ and 0.03, respectively). The observed electronic absorption spectrum of TAPP can be explained on the basis of Gouterman's four-orbital model which considers the two highest occupied and two lowest unoccupied molecular orbitals of the simple Huckel method.[42] Our calculation (Table 2) at the RB3LYP-TD/6-31G(d) level of approximation shows that the HOMO(A1) and HOMO-1(A2) are rigorously degenerate and LUMO(B1) and LUMO-1(B2) are very close in energy, which confirms Gouterman's four-orbital model. Figure 2 displays the four orbitals associated with the electronic transition of the calculated B-band and Q-band absorption, respectively. It shows that orbitals 177 (HOMO $1A_1$) and 176 ($2A_2$) are π orbitals with the electron density being mainly localized on $C_\alpha-C_m-C_\alpha$ atoms and $C_\alpha-C_\beta$ atoms, respectively, while orbitals 179 ($2B_2$) and 178 (LUMO $1B_1$) are π^* orbitals mainly localized on $C_\alpha-C_\beta/C_\alpha-C_m$ and $C_\alpha-C_m/C_\alpha-C_\beta$, respectively, on the basis of our time-dependent density functional theory (TD-DFT) computations and natural orbital analysis. Thus, the experimental 428 nm absorption band (B_x band) (0.41(177→179) + 0.32(176→178) orbital transition) is assigned as the $\pi(C_\alpha-C_m) \rightarrow \pi^*(C_\alpha-C_m)$ and $\pi(C_\alpha-C_\beta) \rightarrow \pi^*(C_\alpha-C_\beta)$ transitions, and the 521 nm absorption band (Q_y band) (0.57(177→178) + 0.42(176→179)) is assigned as the $\pi(C_\alpha-C_m) \rightarrow \pi^*(C_\alpha-C_m)$ transition. Our 416 and 435.7 nm excitation wavelengths used in the resonance Raman experi-

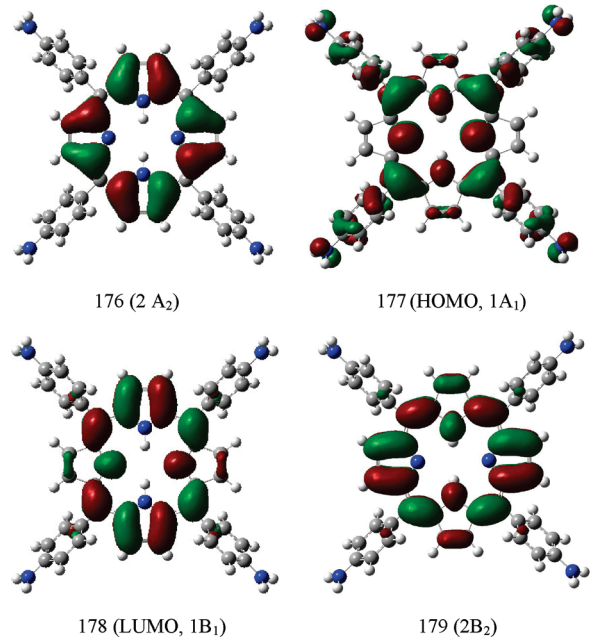

Figure 2. Some highest occupied and lowest unoccupied orbitals and symmetry labels for the B_x and Q_y absorption band of TAPP.

SCHEME 1: Structure and Atom Labeling Scheme of TAPP

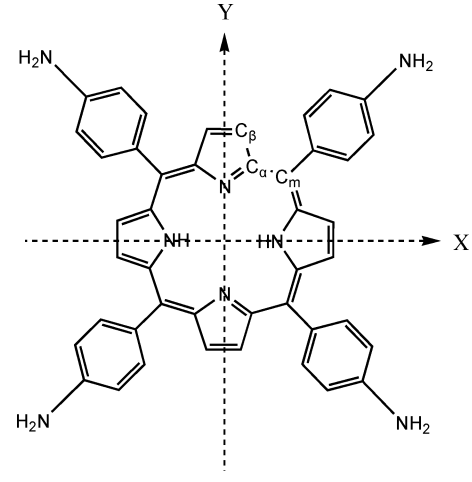

TABLE 3: Experimental and RB3LYP/6-31G(d) Computed Vibrational Frequencies of TAPP (Abbreviated)[a]

	computed (cm^{-1})		experimental (cm^{-1})		
modes	*a*: B3LYP/6-31G*	*b*	FT-Raman	FT-IR	descriptions
			A1		
ν_{10}	1695	1638		1620b	δ(NH) at ph ring
ν_{11}	1670	1614	1606s	1605s	ν(C═C)s at ph ring
ν_{13}	1605	1552	1545vs		$\nu(C_\beta C_\beta + C_m C_\alpha)$
ν_{15}	1565	1513		1512s	δ(CH) at ph ring
ν_{16}	1553	1502	1492w	1470s	$\nu(C_\beta C_\beta)$
ν_{18}	1474	1426	1381	1381	δ(C−H) at ph ring
ν_{19}	1395	1351		1350m	$\nu(C_\alpha C_\beta)$
ν_{22}	1322	1281		1284b	ν(ph-NH_2)
ν_{24}	1266	1227	1238vs	1234vw	$\nu(C_m$−phC)
ν_{25}	1217	1181	1180m	1180vs	δ(CH) at ph ring
ν_{29}	1097	1065	1072w	1068	δ(CH + NH) at ph ring
ν_{31}	1028	999	1001s	984	ν(pyr breath)
ν_{32}	988	961		968	ν(pyr breath)
ν_{36}	861	840		841	δ(pyr deformation) + γ(phCH)
ν_{37}	834	813	820m		δ(pyr deformation)
ν_{39}	824	804		802	$\gamma(C_\beta$H + NH)
ν_{45}	663	650	671m	663	pyr fold + $\gamma(C_\beta$H)
ν_{51}	422	420	416m		phenyl twist
ν_{54}	334	335	333		$\delta(C_\alpha C_m C_\alpha)$as
ν_{56}	216	222	224		pyr tilt
			A2		
ν_{79}	1497	1448	1452s		$\nu(C_m C_\alpha)$as + $\nu(C_\alpha C_\beta)$as
ν_{83}	1366	1323	1329s		$\nu(C_\alpha C_\beta)$as + $\delta(C_\beta$H)
ν_{90}	1169	1134	1138w		δ(NH + C_βH)as
			B1		
ν_{144}	1443	1397	1381s		ν(pry half-ring)s + $\delta(C_\beta$H)s

[a] Note: $b = 0.91a + 87.03$.

ments should be mostly on resonance with the B_x-band absorption of TAPPm while the 397 nm excitation wavelengths are in resonance with the B_y-band absorption and the 514 nm excitation wavelengths are in resonance with the Q_y-band absorption. Since the B_x-band transition (0.41(177→179) + 0.32(176→178) orbital transition) transfers electron density from C_α−C_m into C_α−C_β of porphin ring (see Figure 2), a localized charge transfer nature is expectable for TAPP in a short time upon absorbing 416 or 435.7 nm excitation. The molecular orbital coefficient analysis also supports the electron density redistribution. The Q_y-band transition (0.57(177→178) + 0.42(176→179)) transfers electron density from $C_\alpha C_m$ to $C_\alpha C_\beta$ and from $C_\alpha C_\beta$ to $C_\alpha C_m$ and $C_\beta C_\beta$ of porphin ring (Figure 2); the molecular orbital coefficient analysis also supports the electron density redistribution.

B. Resonance Raman Spectra. The two transitions to the $^1B_1$ and $^1B_2$ states are, respectively, *x* and *y* polarized in the molecular framework, in which *x* and *y* are defined as Scheme 1 shows.

We have carried out DFT calculations for TAPP in order to help elucidate the vibrational bands observed in the experimental FT-Raman and FTIR spectra of TAPP as well as in the resonance Raman spectra of TAPP. Table 3 lists a comparison of the RB3LYP/6-31G(d) calculated vibrational frequencies with experimental FT-Raman and FT-IR values. The notations and assignments of the vibrations are based on the visualization MOLDEN/MIX software, and those previously studied on the Raman spectra of TAPP were used as valuable references.[15,28] The overall agreement between the linear regression scaled DFT calculated vibrational frequencies and the experimental values is good for TAPP. The dihedral angle between the porphin mean plane and the phenyl group in the crystalline state is 81.5°, thus making the crystal structure of free-base porphin have a lower symmetry of the C_{2v} point group instead of the D_{2h} point group.[43] We shall assume in our discussion that the symmetry of the molecule is effectively C_{2v}, and with this background, we are ready to discuss our Raman spectra.

We note first that since our laser line frequencies fall in the electronic absorption region (Figure 1) we may expect to see resonant Raman effects.

For the $\rho\sigma$ element of the polarizability tensor, i.e., eq 4 in the Supporting Information of the C_{2v} TAPP molecule, we shall assume that e^g, e^f, B_x, and Q_y have, respectively, $A_1(z)$, $A_1(z)$, $B_1(x)$, and $B_2(y)$ symmetries and for the normal vibrational resonance Raman scattering both the initial and final electronic states are the ground electronic state, that is, $e^g = e^f$. The excited laser lines at 416 and 435.7 nm fall in the electronic absorption region B_x band (e^r); the transition dipoles of $e^g(A_1(z)) \rightarrow e^r[B(B_1(x))]$ may acquire additional contributions through Herzberg−Teller coupling from the transition dipoles of $e^g(A_1(z)) \rightarrow e^s[Q(B_2(y))]$. From eq 4 in the Supporting Information, the only nonvanishing polarizability tensor elements for the TAPP are

$$\alpha_{xx} = \frac{1}{\hbar}(p_x)^0_{ege^r}(p_x)^0_{e^r e^g}\sum_{v^r}\left(\frac{\langle v^{f(g)}|v^{r(r)}\rangle\langle v^{r(r)}|v^{i(g)}\rangle}{\omega_{e^r v^r;e^g v^i} - \omega_1 - i\Gamma_{e^r v^r}}\right)$$

$$\alpha_{xy} = \frac{1}{\hbar^2}(p_x)^0_{ege^r}\frac{h^k_{e^r e^s}}{\omega_{e^r} - \omega_{e^s}}(p_y)^0_{e^s e^g}\sum_{v^r}\left(\frac{\langle v^{f(g)}|v^{r(r)}\rangle\langle v^{r(r)}|Q_k|v^{i(g)}\rangle}{\omega_{e^r v^r;e^g v^i} - \omega_1 - i\Gamma_{e^r v^r}}\right)$$

$$\alpha_{yx} = \frac{1}{\hbar^2}(p_y)^0_{ege^s}\frac{h^k_{e^s e^r}}{\omega_{e^r} - \omega_{e^s}}(p_x)^0_{e^r e^g}\sum_{v^r}\left(\frac{\langle v^{f(g)}|Q_k|v^{r(r)}\rangle\langle v^{r(r)}|v^{i(g)}\rangle}{\omega_{e^r v^r;e^g v^i} - \omega_1 - i\Gamma_{e^r v^r}}\right) \quad (2)$$

where $(p_x)_{e^f e^r} = \langle e^f|\widehat{p_x}|e^r\rangle$. Since B_x and Q_y have, respectively, Γ_x and Γ_y symmetries, $(p_y)_{e^g e^r}$, $(p_x)_{e^s e^g}$, etc., all equal zero.

Symmetry considerations for α_{xx} nonvanishing require that there must be a displacement ΔQ_k along the normal coordinate

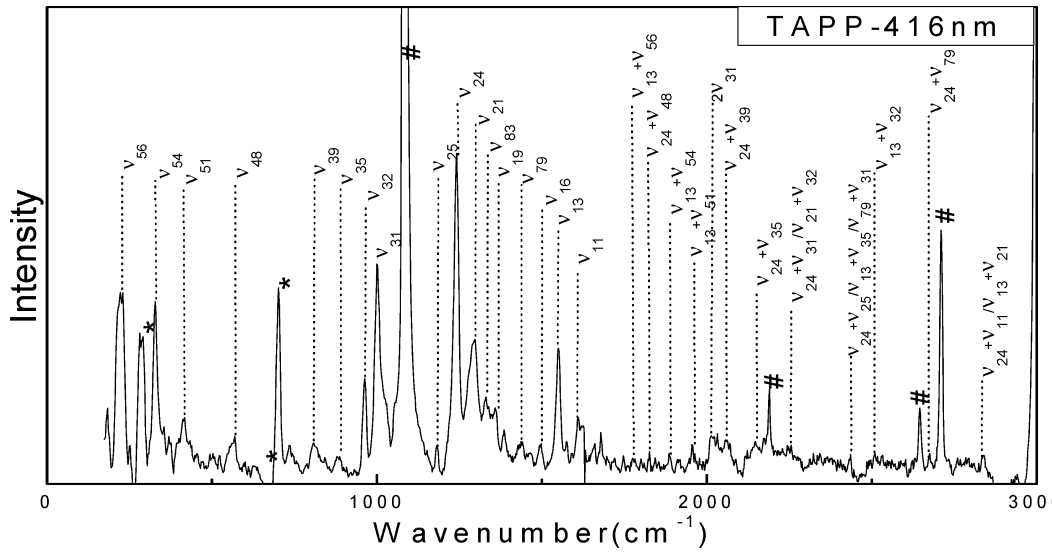

Figure 3. Expanded view of the 416 nm resonance Raman spectrum of TAPP in dichloromethane solvent. The spectra have been intensity corrected and solvent subtracted.

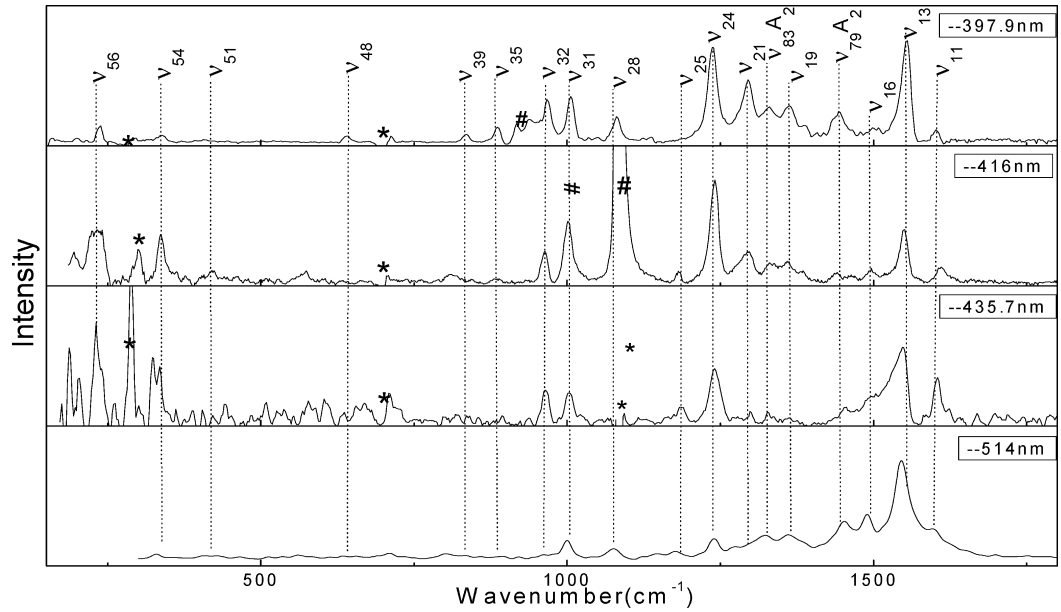

Figure 4. Comparison of the 397.9, 416, 435.7, and 514 nm resonance Raman spectra of TAPP.

which only occurs for totally symmetric modes unless the molecular symmetry is changed in the excited states. That is, both the intermediate and final states $v^{r(r)}$ and $v^{f(g)}$ must be A_1 in order for α_{xx} to not vanish. Figure 3 shows the 416 nm resonance Raman spectrum of TAPP. When the spectrum is excited by the 416 laser line and observed over the 190−3100 cm^{-1} range, it is clear from the figure that only the fundamental bands and their overtones and combinations assignable to A1 symmetry appear in the spectrum. The lines in the 416 nm spectrum are relatively sharp, and there is little indication of the appearance of multiple components. Thus, it appears that the spectrum resulting from excitation into the intense part of the B_x absorption band can be explained in terms of just the α_{xx} term for the TAPP and it is not necessary to invoke the Herzberg−Teller coupling.

On the other hand, since only Q_k modes mix B_x and Q_y, it follows that, for nonzero values of α_{xy} and α_{yx}, requiring $h^k_{e^r e^s} \neq 0$, simultaneously at least one v^r term $\langle v^{f(g)}|v^{r(r)}\rangle\langle v^{r(r)}|Q_k|v^{i(g)}\rangle$ or $\langle v^{f(g)}|Q_k|v^{r(r)}\rangle\langle v^{r(r)}|v^{i(g)}\rangle \neq 0$ in the sum. For the integral $h^k_{e^r e^s}$ unequal to zero, the irreducible representation Γ_{Q_k} of the vibrational fundamental with normal coordinate Q_k must be contained in the direct product of the irreducible representations of the states $|e^r\rangle$ and $|e^s\rangle$, that is, $\Gamma_{Q_k} \subset \Gamma_{B_x} \times \Gamma_{Q_y} = B_1 \times B_2$, accordingly leads to $\Gamma_{Q_k} = A_2$, and for the $\langle v^{f(g)}|v^{r(r)}\rangle\langle v^{r(r)}|Q_k|v^{i(g)}\rangle \neq 0$ or $\langle v^{f(g)}|Q_k|v^{r(r)}\rangle\langle v^{r(r)}|v^{i(g)}\rangle \neq 0$, the irreducible representation of $v^{r(r)}$ and $v^{f(g)}$ must be $\Gamma v^{r(r)} = \Gamma v^{f(g)} = \Gamma_{Q_k} = A_2$. Depending upon the extent of the coupling of the electronic and vibrational states, the Raman spectrum could be extremely complex. Egawa et al. also reported that A_2 modes should be considered as the best means for elucidating vibronic characters of absorption bands of porphyrins.[23]

Figure 4 displays the comparison of the 397.9, 416, 435.7, and 514 nm resonance Raman spectra of TAPP in dichloromethane solvent. The dashed lines in Figure 4 indicate the correlation of 16 A_1 type fundamental vibrational modes labeled as ν_{11}, ν_{13}, ν_{16}, ν_{17}, ν_{19}, ν_{21}, ν_{24}, ν_{25}, ν_{31}, ν_{32}, ν_{35}, ν_{39}, ν_{48}, ν_{51}, ν_{54}, and ν_{56} and two nontotally symmetric vibrational mode $\nu_{79}[\nu(C_mC_\alpha)as + \nu(C_\alpha C_\beta)as]$ stretch and $\nu_{83}[(C_\alpha\ C_\beta)as$ stretch $+ \delta(C_\beta H)]$ of A_2 type in 397.9, 416, 435.7, and 514 nm resonance Raman spectra. The nontotally symmetric modes ν_{79}

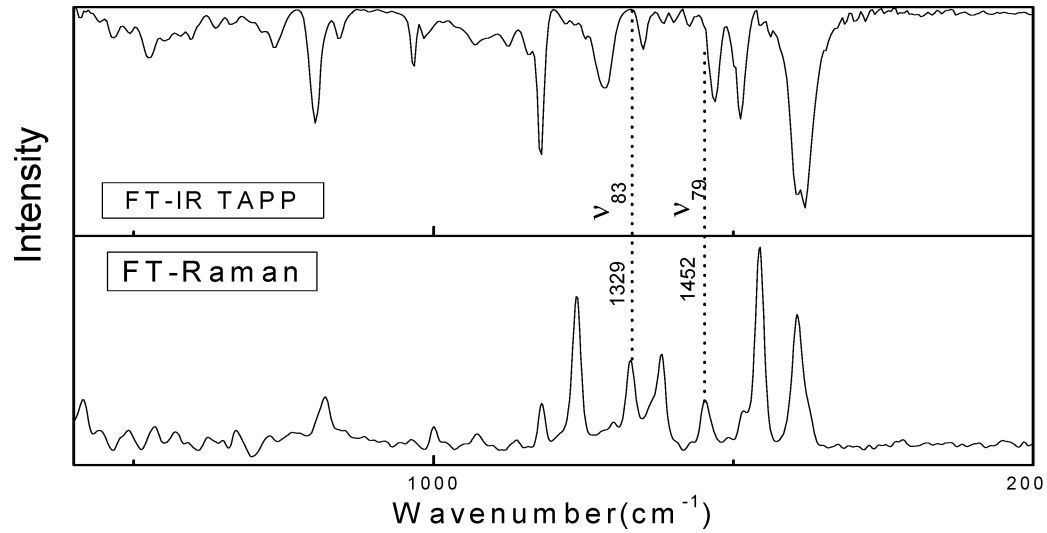

Figure 5. FT-IR (top) and FT-Raman (bottom) spectra of TAPP.

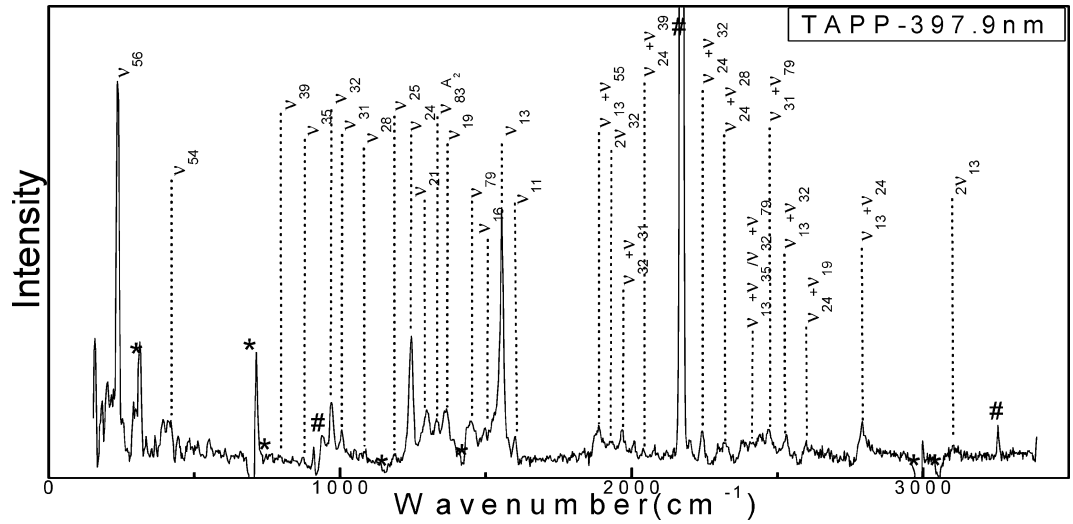

Figure 6. Expanded view of the 397.9 nm resonance Raman spectrum of TAPP in dichloromethane solvent. The spectra have been intensity corrected and solvent subtracted (asterisks mark regions where solvent subtraction artifacts are present, and pound signs stand for residual uncertain laser). The tentative assignments to the larger Raman band features are also shown.

and ν_{83} are also active in FT-Raman spectroscopy but absent in the FT-IR spectrum (see Figure 5), which confirm the A_2 symmetry assignment of these modes according to the C_{2v} point group. The 416 and 435.7 nm laser frequency lies in a region in which the continuum states of the potential surface of electronic state Q_y overlap the discrete levels of state B_x, the 397.9 nm laser frequency lies in a overlap region of the continuum states B_x and the discrete state B_y, and the 514 nm laser frequency lies in an overlap region of the continuum state Q_x and the discrete state Q_y. In such a region, the adiabatic approximation described earlier is expected to fail and the mixing of vibronic levels through nonadiabatic interactions involving the nuclear kinetic energy operator becomes significant, which may lead to conical intersection between different potential energy surfaces (PES) and alter the photoreaction channel. This has already been verified by A. Marcelli et al. for time-resolved photoexcitation in the Soret band with pulses of femtosecond duration experiment.[44] The 397.9, 416, 435.7, and 514 nm resonance Raman spectra of TAPP indicate that, while most of the excited state structural dynamics are along the total symmetry vibrational reaction coordinates, it also moves along the nontotally symmetric reaction coordinate significantly, indicating the existence of the Franck−Condon region vibronic coupling between the B_y, B_x, and Q_y electronic states. Figure 4 also shows that, while the vibrational modes in wavenumber and in description for different resonance Raman spectra are very similar, the intensity patterns are very different. It is observed that the closer the laser excitation wavelengths lie to 428 nm, the weaker is the intensity of the A_2 nontotally symmetric vibrational mode $\nu_{79}[\nu(C_mC_\alpha)as + \nu(C_\alpha C_\beta)as]$ stretch and $\nu_{83}[(C_\alpha\ C_\beta)as\ stretch + \delta(C_\beta H)]$, indicating the weaker coupling or less overlap between B_y and B_x states or B_x and Q_y states.

Figures 3 and 6−8 present an expanded view of the resonance Raman spectrum of TAPP obtained with 397.9, 416, 435.7, and 514 nm excitations, respectively, with tentative vibrational assignments indicated in the spectra and also given in Table 3. We note that the intensity of some Raman bands in the spectrum may have contributions from several Raman bands that have very close Raman shifts due to the limited resolution of the solution phase spectrum, and therefore, the Raman band labels in Figures 3 and 6−8 only indicate the largest Raman band contributions to each Raman feature.

The spectra of TAPP at 416 and 435.7 nm are resonant with the B_x-band absorption and show several progressions of overtones and combination bands. The peak positions and

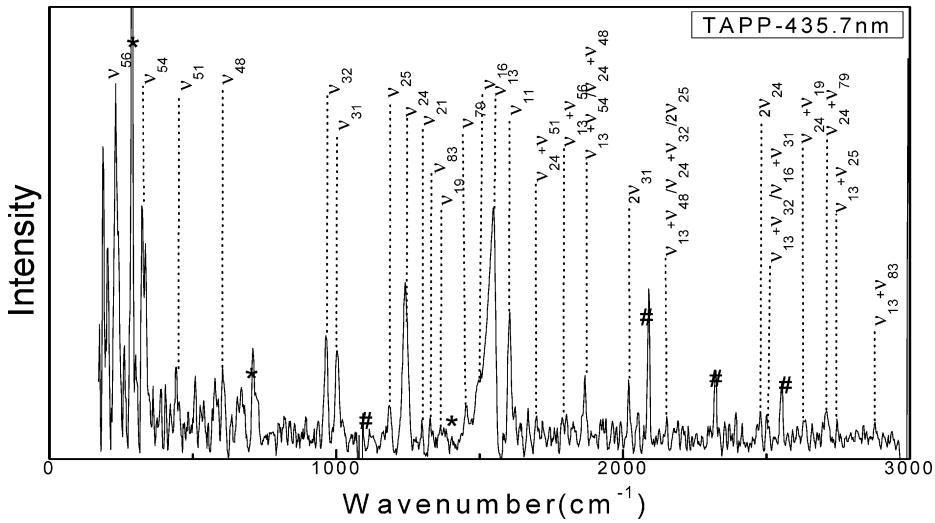

Figure 7. Expanded view of the 435.7 nm resonance Raman spectrum of TAPP in dichloromethane solvent. The spectrum has been intensity corrected and solvent subtracted.

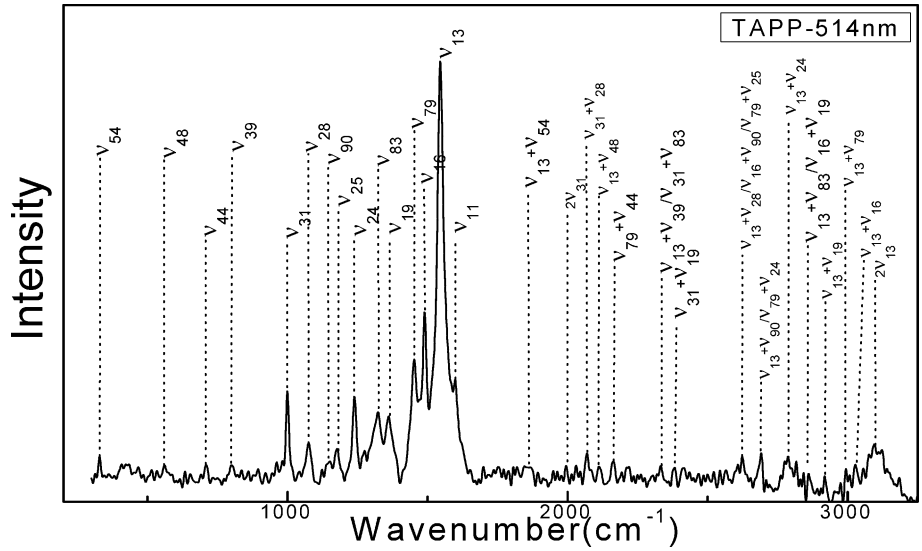

Figure 8. Expanded view of the 514 nm resonance Raman spectrum of TAPP. The spectrum has been intensity corrected and solvent subtracted. The tentative assignments to the larger Raman band features are also shown.

intensities (absolute Raman cross sections) for the 397.9, 416, and 435.7 nm spectra indicated in Figures 3 and 6−7 are given in Table 4. These total absolute cross sections have been calculated from the directly measured relative differential cross sections as discussed in refs 45−47. From Figures 3 and 7 and Table 4, the largest progression in these B_x-band resonant spectra is the nominal porphin ring $C_\beta{=}C_\beta + C_mC_\alpha$ stretch fundamental, overtones, and combination bands ν_{13}(1545 cm^{-1}). The next largest progression is the nominal C_m-ph stretch fundamental plus combination band ν_{24}(1240 cm^{-1}). There are also two smaller combination bands made up of the nominal porphin ring breath ν_{31}(999 cm^{-1}) + ν_{32} (962 cm^{-1}) fundamentals. Most importantly, two nontotally symmetric vibrational mode $\nu_{79}[\nu(C_mC_\alpha)$as + $\nu(C_\alpha C_\beta)$as] stretch and $\nu_{83}[(C_\alpha\ C_\beta)$as stretch + $\delta(C_\beta H)]$ in A_2 irreducible representative occurs in the B_x- and B_y-band resonant spectra. This suggests that, upon photoexcitation in the B_x-band absorption, TAPP undergoes larger motions along the symmetric vibrational relaxation coordinates of porphin ring $C_\beta{=}C_\beta$ + C_mC_α stretch, C_m-ph stretch, and porphin ring breath and simultaneously along the asymmetric (C_mC_α)as stretch, $(C_\alpha C_\beta)$as stretch, and $\delta(C_\beta H)$ vibrational

TABLE 4: Experimental Resonance Raman Intensities for TAPP in Dichloromethane Solution

descriptions	frequency (cm^{-1})	397.9 nm ($\times10^{-8}$)	416 nm ($\times10^{-8}$)	435.7 nm ($\times10^{-8}$)
ν_{13}	1555	133	25	141
$2\nu_{13}$	3110	14		
$\nu_{13} + \nu_{24}$	2799	16		4
$\nu_{13} + \nu_{32}$	2524	12	6	3
$\nu_{13} + \nu_{19}$	2920	3		
$\nu_{13} + \nu_{25}$	2746	5	1	2
ν_{24}	1244	65	76	77
$\nu_{24} + \nu_{32}$	2213	19		3
$\nu_{24} + \nu_{19}$	2609	4		3
$\nu_{24} + \nu_{25}$	2435	9	7	3
ν_{32}	969	23	11	35
$2\nu_{32}$	1938	10	3	2
$\nu_{32} + \nu_{31}$	1975	17		3
ν_{25}	1191	9	4	17
ν_{19}	1365	15	17	8
ν_{31}	1006	6	65	41
ν_{79}	1446	61	16	15
$\nu_{79} + \nu_{31}$	2452	12	7	

relaxation processes leading to the Q_y state. Figures 3 and 7 show that the porphin ring C_β═C_β + C_mC_α and C_m—ph bond lengthenings dominate the S_3 excited state structural dynamics of the TAPP molecule; the result is in consistency with the facts that the B_x-band electron transition weakens the C_m—C_α bond and strengthens the C_β═C_β bonds (see Figure 2 and Table 1).

Hence, S_3 state excitation largely changes the strength of the C_β═C_β, C_m—C_α, and C_m—ph bonds but has little effect on either the N—C and N—H bonds of the protonated rings or the phenyl substituents. It is worth stressing that these changes in bonding strength, which accompany excitation to the high electronic state, correspond to the changes in force constants which are extremely small but that the overall effect of excitation on the chemical reactivity of the system is significant. For example, these systems are reducing agents in the lower energy excited state and have been extensively investigated as components in solar-energy conversion systems.[45−47] It is apparent that in the excited state the energy is not localized in small regions of the conjugated system but is spread throughout the system. This gives minor changes in bond lengths and large energies concerned motions of many atoms within the molecules, in contrast to the large changes in bonding within localized regions which are observed in the case of benzophenone,[48,25] for example. This delocalization would, of course, be expected for any large aromatic molecule, but the relative ease of isotopic substitution and the extensive database, now available, make the porphyrins ideal systems for the investigation of photodynamics of different excited states.

The 514 nm spectrum (Figure 8) is resonant with the Q_y-band absorption and shows a distinctly different pattern of Raman intensities from the B-band resonant spectra. The strongest feature in the 514 nm spectrum is the C_β═C_β + C_mC_α stretch fundamental ν_{13}. The second strongest feature is the nominal $\nu(C_mC_\alpha)$as + $\nu(C_\alpha C_\beta)$as stretch ν_{79} which we assign as the A_2 irreducible representative. This suggests that, upon photoexcitation in the Q_y-band absorption region, TAPP undergoes larger motions along the reaction coordinates of porphin ring C_β═C_β + C_mC_α stretch and $\nu(C_mC_\alpha)$as + $\nu(C_\alpha C_\beta)$as stretch. It appears that the porphin ring C_β═C_β + C_mC_α dominates the S_2 excited state structural dynamics of the TAPP molecule; the result is in consistency with the facts that the Q_y-band electron transition passes one electron from $C_\alpha C_m$ to $C_\alpha C_\beta$ and from $C_\alpha C_\beta$ to $C_\alpha C_m$ and $C_\beta C_\beta$ based on Figure 2 and the molecular orbital coefficient analysis. Vibronic coupling intensities of A_2 symmetry modes ν_{79} and even its overtones $2\nu_{79}$ and combination tones presented in the 514 nm resonance Raman spectrum suggest that the S_2 excited state structural dynamics involves the vibronic coupling of the S_2 state to S_1 excited electronic states due to nonzero contribution from the D-term in the vibrational transition polarizability tensor $(\alpha_{\rho\sigma})_{e^fv^f;e^gv^i}$.

C. Resonance Raman Depolarization Ratios. Measurements of depolarization ratios can give information about the symmetry of electronic states. Depolarization ratios for the stronger Raman lines were measured for TAPP at 416 nm. Due to the difficulty of these experiments (the polarizer strongly attenuates the already weak scattered light), measurements were not attempted at other wavelengths. The depolarization ratio of the C_β═C_β + C_mC_α stretching fundamental ν_{13}, C_m—ph stretch fundamental ν_{24}, porphin ring breath ν_{32}, porphin ring breath ν_{31}, and $\nu(C_mC_\alpha)$as + $\nu(C_\alpha C_\beta)$as asymmetric stretching fundamental ν_{79} were found to be 0.33, 0.35, 0.24, 0.64, and 0.15 (all ±0.02), respectively. The values of depolarization ratios vary with frequency and exhibit polarization dispersion. This is in contrast to depolarization ratios involving just one resonant electronic state which show no dispersion (equal to l/3). This polarization dispersion, a significant difference from l/3, suggests that the majority of the resonant enhancement of the stretching fundamental is contribute from the different component of the electronic transitions (B_x and B_y) and may evoke vibronic couplings from the Q band. On the other hand, band features of ν_{79} in the 416 nm excited spectrum seem unlikely as A_1 modes for its anomalously polarized Raman line. Egawa et al. also reported that A_2 modes should be considered as the best means for elucidating vibronic characters of absorption bands of porphyrins.[23]

D. The B_x-Band TAPP Photodissociation Dynamics and Comparison to Previous Work on Porphyrin. The early excited-state dynamics of porphyrin have been explored by using ultrafast time-resolved spectroscopy techniques.[49,50] The experimental results revealed the relaxation dynamics of porphyrin. In the relaxation process, vibrationally excited B → Q_y internal conversion occurs in the 40−50 fs time regime and Q_y → Q_x internal conversion with a time constant of 150 fs. This time is unresolvably short in H_2TPP.[49]

The first conclusion that we can draw from our data is that the population decay from the Soret band to levels of the Q_y and from the Q_y band to levels of the Q_x takes place very rapidly. Our resonance Raman spectroscopy studies provide a possible way to clarify whether a vibronic coupling between the two states with different irreducible representations exists in the Franck−Condon region or not. Resonance Raman mostly reflect the dynamics only at short times, where the nuclei have not yet moved far from the Franck−Condon region, since the overlaps $\langle f|0(t)\rangle$ which determine the calculated resonance Raman intensities reach their maxima at times in the 5−10 fs range for most of the observed transitions. Also, 10 fs is short compared with the recurrence times of any of the active vibrations. By discerning some antisymmetric vibrational modes, one can identify whether there is any geometry distortion motion occurring in the FC region in the 10 fs short-time dynamics.[51,52] For example, resonance Raman studies on ethylene have demonstrated that strong vibronic coupling exists in the V state and the torsional vibration is the primary active mode in the N → V ($\pi\pi^*$) transition.[51,52]

Our resonance Raman spectra of TAPP show that there are A_2 nontotally symmetric vibrational modes appearing in FC region for TAPP in B- and Q_y-band excitation. This demonstrates that when the wave packet leaves from the FC region, the molecule evolves along the total (and/or the local) symmetry modes for TAPP and nontotally symmetric motions $\nu(C_mC_\alpha)$as + $\nu(C_\alpha C_\beta)$as asymmetric stretch appear in or near the FC region. This clearly indicates that vibronic coupling occurs between the B_x state and Q_y state and that the B_x/Q_y conical intersection must occur in the region relatively far beyond FC. It appears that our short-time dynamics supports the picture that the TAPP molecule initially moves on the potential surface that is along totally symmetry vibrational modes and, then, evolves into the B_x/Q_y conical intersection channels in tens of femtoseconds.

A lifetime of tens of femtoseconds for the Soret band is in good agreement with the calculation based on fluorescence quantum yields[49] and also appears consistent with the measurement and interpretation of Fong and co-workers,[53] who reported an estimated internal conversion (IC) rate of tens of femtoseconds following excitation at 398 nm in chloroform of H_2TPP.

The time constant dramatic decrease from ~50 fs in ZnTPP,[55] as well as in other metalloporphyrins,[54] to 10 fs in TAPP is related to the decrease of the energy gap $\Delta E(B_x-Q_y)$ between electronic states. The energy gap between B_x and Q_y of H_2P in

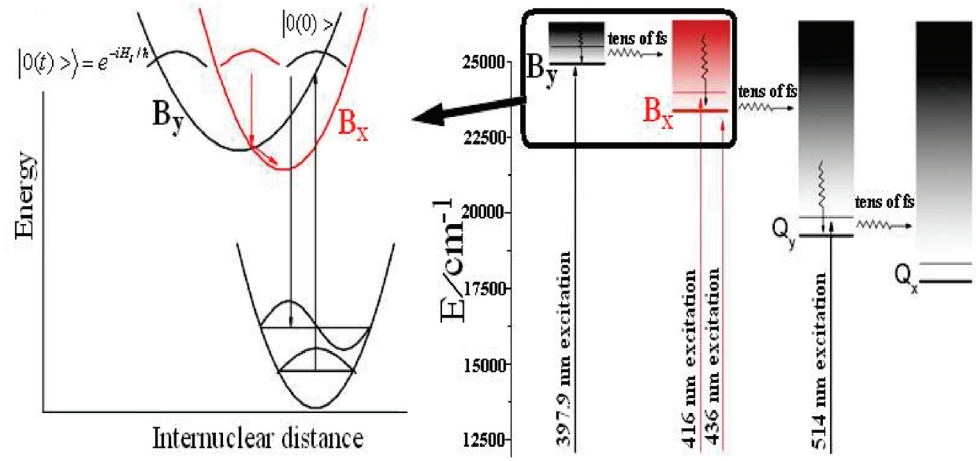

Figure 9. Schematic diagram of the energy relaxation dynamics of TAPP in dichloromethane solution. (right) The solid horizontal lines are located at the energies of bands in the absorption spectrum. (left) The time-dependent interpretation of Raman scattering $B_y \rightarrow B_x$ internal conversion relaxation dynamics of TAPP in dichloromethane solution.

benzene/cyclohexane 1:10 is ~6100 cm^{-1}, in ZnTPP, the B(0,0)−Q(0,0) gap is ~6670 cm^{-1}, and in TAPP, the B_x and Q_y gap is 4189 cm^{-1} and no additional singlet states between B_x and Q_y contribute to the decay.[44] According to the energy gap law, the time constant increases exponentially with increasing energy gap. This relation has been invoked in previous analyses of the variation in Soret lifetimes with environment.[44] If the correlations of rate constant vs energy gap, which are plotted in ref 44, are extrapolated to smaller energy gap, both show that a femtosecond rate would be expected for an energy gap of 4189 cm^{-1}.

Similarly, the nontotally symmetric vibrational mode in A_2 is an irreducible representative of ν_{79} [$\nu(C_mC_\alpha)$as + $\nu(C_\alpha C_\beta)$as] and even its overtones $2\nu_{79}$ and combination tones, which arise from Q_x-band contribution to the Q_y excited states resonance Raman spectrum. It shows that the relaxation short-time dynamics of the TAPP molecule for the excited Q_y state initially moves on the potential surface that is along totally symmetry vibrational modes and, then, evolves into the Q_y/Q_x conical intersection channels in tens of femtoseconds short time. Again, the short times in transient absorption spectrum experiment for $Q_y \rightarrow Q_x$ internal conversion have been estimated in the H_2TPP and more complex porphyrin derivatives to be tens of femtoseconds.[44]

The differences between experimental oscillator strength and calculated oscillator strength in Table 1 could be explained by the vibronic coupling between adjacent excited states. For example, 397 nm excitation of TAPP to the S_4 state and ultrafast internal conversion of the S_4 to S_3 state by nontotally symmetric vibration of A_2 type contribute intensity to the S_3 state. Consequently, it decreases the oscillator strength of the S_4 state and increases the oscillator strength of the S_3 state. This makes the oscillator strengths of the S_4 and S_3 states less and more, respectively, than the calculated values. From the final outcome of experimental oscillator strength, we can show an order for coupling strength between the states: $S_4/S_3 \gg S_3/S_2 = S_2/S_1$.

The pathways and time scales for relaxation of TAPP in dichloromethane as discussed in the preceding paragraphs are represented schematically in Figure 9. At time zero, interaction with the 397 nm laser radiation, ground state TAPP with A_1 molecular symmetry was excited and results in a vertical transition to the S_4 (B_y) state in the FC region through the involvement of the electronic transition moment; then, it reorganized and relaxed with B_2 molecular symmetry. The wave packet $|0(t)\rangle$ is now under the influence of a Hamiltonian H, and it begins to move with time from its initial position which is indicated by a solid line labeled with $|0(0)\rangle$ in the left part of Figure 9 and then reaches the left-hand side of the excited state potential. The wave packet is then reflected and oscillation between the two side potential in the B_y state, but the strength is gradually damped out by the damping function $\exp[-\Gamma t/\hbar]$. During the process of propagation with time, the wave packet $|0(t)\rangle$ crosses regions of large overlap with the wave function $|f\rangle$ in the ground electronic state. The Raman overlap $|\langle f|0(t)\rangle| \times \exp[-\Gamma t/\hbar]$ therefore has a maximum at this point of time, and the square of the half-Fourier transform of the overlap (see eq 1 in the Experimental and Computational Methods section) produces the Raman scattering excitation profile which is given in Table 4. Symmetry considerations require that such an oscillation can occur only for totally symmetric modes which do not alter the molecular symmetry. Simultaneously, when the wave packet approached the intersection of B_y and B_x states, only the nontotally symmetric modes worked to alter the shape of the potential energy surface from B_2 to B_1 symmetry, and then induces the ultrafast IC happens, decaying to the B_x state, and then the wave packet is reflected and oscillation between the two side potential in B_x state, the Raman overlap $|\langle f|0(t)\rangle| \times \exp[-\Gamma t/\hbar]$ in this situation produce the A_2 vibronic coupling intensities. The same analysis could be applied to the other process in Figure 9.

Further investigations are needed to better clarify the conical intersection between the multiple complex excited electronic states. The B state is really complex and may contain other trivial excited states; here, we have found one higher energy excited state that couples with B_x, which was predicted by Egawa et al. previously.[23] The short-time dynamics in terms of the internal coordinate changes would also be useful to quantitatively examine how the Franck−Condon region geometry changes correlate with the possible conical intersection between the initial B_x state and other excited states. Experiments directing how different substituents influence the photodissociation dynamics and photochemistry of porphyrins are still in progress.

Conclusion

RRs of 397.9, 416, 435.7 (B band), and 514 nm (Q_y band) excitation wavelength were acquired for TAPP, and the Raman

effect of relaxation dynamics was analyzed according to Herzberg−Teller (vibronic coupling) contributions. Our results indicate that the short-time $S_0 \rightarrow S_3$ photorelaxation dynamics of TAPP have substantial multidimensional character mainly in the nominal $C_\beta{=}C_\beta + C_mC_\alpha$ stretching, the nominal $C_m{-}$ph stretch mode, and the nominal porphin ring breath, with smaller contributions from the nominal $C_mC_\alpha + C_\alpha C_\beta$ asymmetric stretch and the nominal $C_\alpha C_\beta$ stretch, while that for the $S_0 \rightarrow S_2$ electronic state is predominantly along the porphin ring $C_\beta{=}C_\beta$ stretch. The overall picture of relaxation dynamics for TAPP is presented, and the detailed short-time dynamics for internal conversion and the vibronic coupling mechanisms are interpreted with the time-dependent wave packet theory. The vibrationally excited B_x (S_3) $\rightarrow Q_y$ electronic relaxation dynamics occurs in tens of femtoseconds. The time occurs shorter compared to porphyrin and H_2TPP.

Acknowledgment. This work was supported by grants from NSFC (nos. 20703038 and 20803066), the National Basic Research Program of China (2007CB815203), and NSFZ (nos. Y407245 and R405465). H.W. wishes to acknowledge the referees for their contributions in making this a better paper.

Supporting Information Available: Theory of Raman scattering, procedures for calculation of total absolute cross sections of TAPP, RR spectra of the TAPP in parallel and perpendicular polarization, depolarization ratios calculated from the RRs, and experimental and RB3LYP/6-31G(d) computed vibrational frequencies of TAPP. This material is available free of charge via the Internet at http://pubs.acs.org.

References and Notes

(1) Miller, R. A.; Presley, A. D.; Francis, M. B. *J. Am. Chem. Soc.* **2007**, *129*, 3104.
(2) Ahn, T. K.; Kim, K. S.; Kim, D. Y.; Noh, S. B.; Aratani, N.; Ikeda, C.; Osuka, A.; Kim, D. *J. Am. Chem. Soc.* **2006**, *128*, 1700.
(3) Purschwitz, J.; Mueller, S.; Kastner, C.; Schoser, M.; Haas, H.; Espeso, E. A.; Atoui, A.; Calvo, A. M.; Fischer, R. *Curr. Biol.* **2008**, *18*, 255.
(4) Kumble, R.; Palese, S.; Lin, V. S. Y.; Therien, M. J.; Hochstrasser, R. M. *J. Am. Chem. Soc.* **1998**, *120*, 11489.
(5) Iwamura, M.; Takeuchi, S.; Tahara, T. *J. Am. Chem. Soc.* **2007**, *129*, 5248.
(6) Song, H. E.; Kirmaier, C.; Taniguchi, M.; Diers, J. R.; Bocian, D. F.; Lindsey, J. S.; Holten, D. *J. Am. Chem. Soc.* **2008**, *130*, 15636.
(7) Baskin, J. S.; Yu, H.-Z.; Zewail, A. H. *J. Phys. Chem. A* **2002**, *106*, 9837.
(8) Zhong, Q. H.; Wang, Z. H.; Liu, Y. Q.; Zhu, Q. H.; Kong, F. A. *J. Chem. Phys.* **1996**, *105*, 5377.
(9) He, Y.; Xiong, Y. J.; Zhu, Q. H.; Kong, F. A. *Acta Phys.-Chim. Sin.* **1999**, *15*, 636.
(10) Even, U.; Magen, J.; Jortner, J.; Friedman, J.; Levanon, H. *J. Chem. Phys.* **1982**, *77*, 4374.
(11) Schweitzer-Stenner, R. *Vib. Spectrosc.* **2006**, *42*, 98.
(12) Saini, G. S. S.; Chaudhury, N. K.; Verma, A. L. *Photochem. Photobiol.* **1992**, *55*, 815.
(13) Saini, G. S. S.; Sharma, S.; Kaur, S.; Tripathi, S. K.; Mahajan, C. G. *Spectrochim. Acta, Part A* **2005**, *61*, 3070.
(14) Saini, G. S. S. *Spectrochim. Acta, Part A* **2006**, *64*, 981.
(15) Saini, G. S. S.; Sharma, A.; Singh, S.; Abbas, J. M.; Tripathi, S. K.; Kaur, S.; Mahajan, C. G.; Thanga, H. H.; Verma, A. L. *J. Raman Spectrosc.* **2007**, *38*, 1561.
(16) Bell, S. E. J.; Alobaidi, A. H. R.; Hegarty, M.; Hester, R. E.; McGarvey, J. J. *J. Phys. Chem.* **1993**, *97*, 11599.
(17) Bell, S. E. J.; Alobaidi, A. H. R.; Hegarty, M. J. N.; McGarvey, J. J.; Hester, R. E. *J. Phys. Chem.* **1995**, *99*, 3959.
(18) Bell, S. E. J.; Aakeroy, C. B.; Alobaidi, A. H. R.; Hegarty, J. N. M.; McGarvey, J. J.; Lefley, C. R.; Moore, J. N.; Hester, R. E. *J. Chem. Soc., Faraday Trans.* **1995**, *91*, 411.
(19) Bell, S. E. J. *Analyst* **1996**, *121*, R107.
(20) Oakes, R. E.; Bell, S. E. J. *J. Phys. Chem. A* **2003**, *107*, 10953.
(21) Binstead, R. A.; Crossley, M. J.; Hush, N. S. *Inorg. Chem.* **1991**, *30*, 1259.
(22) Binstead, R. A.; Hush, N. S. *J. Phys. Chem.* **1993**, *97*, 13172.
(23) Egawa, T.; Suzuki, N.; Dokoh, T.; Higuchi, T.; Shimada, H.; Kitagawa, T.; Ishimura, Y. *J. Phys. Chem. A* **2004**, *108*, 568.
(24) Li, X. Y.; Czernuszewicz, R. S.; Kincaid, J. R.; Su, Y. O.; Spiro, T. G. *J. Phys. Chem.* **1990**, *94*, 31.
(25) Li, X. Y.; Zgierski, M. Z. *J. Phys. Chem.* **1991**, *95*, 4268.
(26) Starovoitova, V.; Budarz, T. E.; Wyllie, G. R. A.; Scheidt, W. R.; Sturhahn, W.; Alp, E. E.; Prohofsky, E. W.; Durbin, S. M. *J. Phys. Chem. B* **2006**, *110*, 13277.
(27) Minaev, B.; Wang, Y. H.; Wang, C. K.; Luo, Y.; Agren, H. *Spectrochim. Acta, Part A* **2006**, *65*, 308.
(28) Zhang, Y. H.; Ruan, W. J.; Li, Z. Y.; Wu, Y.; Zheng, J. Y. *Chem. Phys.* **2005**, *315*, 201.
(29) Toivonen, T. L. J.; Hukka, T. I.; Cramariuc, O.; Rantala, T. T.; Lemmetyinen, H. *J. Phys. Chem. A* **2006**, *110*, 12213.
(30) Kwok, W. M.; Phillips, D. L. *Chem. Phys. Lett.* **1995**, *235*, 260.
(31) Trulson, M. O.; Mathies, R. A. *J. Chem. Phys.* **1986**, *84*, 2068.
(32) Li, B. L.; Myers, A. B. *J. Phys. Chem.* **1990**, *94*, 4051.
(33) Lee, S. Y.; Heller, E. J. *J. Chem. Phys.* **1979**, *71*, 4777.
(34) Heller, E. J.; Sundberg, R. L.; Tannor, D. J. *J. Phys. Chem.* **1982**, *86*, 1822.
(35) Myers, A. B. *Laser Techniques in Chemistry*; Wiley: New York, 1995.
(36) Myers, A. B.; Mathies, R. A. *Biological Applications of Raman Spectroscopy*; Wiley: New York, 1987; Vol. 2.
(37) Long, D. A. *The Raman Effect: A Unified Treatment of the Theory of Raman Scattering by Molecules*; John Wiley & Sons Ltd: Chichester, England, 2002.
(38) Becke, A. D. *J. Chem. Phys.* **1986**, *84*, 4524.
(39) Lee, C. T.; Yang, W. T.; Parr, R. G. *Phys. Rev. B* **1988**, *37*, 785.
(40) Frisch, M. J.; Trucks, G. W.; Schlegel, H. B.; Scuseria, G. E.; Robb, M. A.; Cheeseman, J. R.; Montgomery, J. A., Jr.; Vreven, T.; Kudin, K. N.; Burant, J. C.; Millam, J. M.; Iyengar, S. S.; Tomasi, J.; Barone, V.; Mennucci, B.; Cossi, M.; Scalmani, G.; Rega, N.; Petersson, G. A.; Nakatsuji, H.; Hada, M.; Ehara, M.; Toyota, K.; Fukuda, R.; Hasegawa, J.; Ishida, M.; Nakajima, T.; Honda, Y.; Kitao, O.; Nakai, H.; Klene, M.; Li, X.; Knox, J. E.; Hratchian, H. P.; Cross, J. B.; Adamo, C.; Jaramillo, J.; Gomperts, R.; Stratmann, R. E.; Yazyev, O.; Austin, A. J.; Cammi, R.; Pomelli, C.; Ochterski, J. W.; Ayala, P. Y.; Morokuma, K.; Voth, G. A.; Salvador, P.; Dannenberg, J. J.; Zakrzewski, V. G.; Dapprich, S.; Daniels, A. D.; Strain, M. C.; Farkas, O.; Malick, D. K.; Rabuck, A. D.; Raghavachari, K.; Foresman, J. B.; Ortiz, J. V.; Cui, Q.; Baboul, A. G.; Clifford, S.; Cioslowski, J.; Stefanov, B. B.; Liu, G.; Liashenko, A.; Piskorz, P.; Komaromi, I.; Martin, R. L.; Fox, D. J.; Keith, T.; Al-Laham, M. A.; Peng, C. Y.; Nanayakkara, A.; Challacombe, M.; Gill, P. M. W.; Johnson, B.; Chen, W.; Wong, M. W.; Gonzalez, C.; Pople, J. A. *Gaussian 03*; Gaussian, Inc.: Pittsburgh, PA, 2003.
(41) Champion, P. M.; Korenowski, G. M.; Albrecht, A. C. *Solid State Commun.* **1979**, *32*, 7.
(42) Gouterman, M. *J. Mol. Spectrosc.* **1961**, *6*, 138.
(43) Hamor, M. J.; Hamor, T. A.; Hoard, J. L. *J. Am. Chem. Soc.* **1964**, *86*, 1938.
(44) Marcelli, A.; Foggi, P.; Moroni, L.; Gellini, C.; Salvi, P. R. *J. Phys. Chem. A* **2008**, *112*, 9.
(45) Balzani, V.; Credi, A.; Venturi, M. *ChemSusChem* **2008**, *1*, 33.
(46) Gust, D.; Moore, T. A.; Moore, A. L. *Acc. Chem. Res.* **2001**, *34*, 40.
(47) Gust, D.; Moore, T. A.; Moore, A. L. *Acc. Chem. Res.* **2001**, *34*, 40.
(48) Tahara, T.; Hamaguchi, H.; Tasumi, M. *J. Phys. Chem.* **1987**, *91*, 5875.
(49) Baskin, J. S.; Yu, H.-Z.; Zewail, A. H. *J. Phys. Chem. A* **2002**, *106*, 9837.
(50) Marcelli, A.; Foggi, P.; Moroni, L.; Gellini, C.; Salvi, P. R. *J. Phys. Chem. A* **2008**, *112*, 1864.
(51) Ziegler, L. D.; Hudson, B. S. *J. Chem. Phys.* **1983**, *79*, 1197.
(52) Gao, P.-C.; Wang, H.-g.; Pei, K.-M.; Zheng, X. *Chem. Phys. Lett.* **2007**, *445*, 173.
(53) Zhong, Q.; Wang, Z.; Liu, Y.; Zhu, Q. H.; Kong, F. A. *J. Chem. Phys.* **1996**, *105*, 5377.
(54) Zhang, X.; Wasinger, E. C; Muresan, A. Z.; Attenkofer, K.; Jennings, G.; Lindsey, J. S.; Chen, L. X. *J. Phys. Chem. A* **2007**, *111*, 11736.
(55) Yu, H.-Z.; Baskin, J. S.; Zewail, A. H. *J. Phys. Chem. A* **2002**, *106*, 9845.

JP1000978